10-15-2019

Pressure effect on an ocean-based humidification-dehumidification desalination process

Yingchen Yang
The University of Texas Rio Grande Valley, yingchen.yang@utrgv.edu

Recommended Citation

Yang, Yingchen. "Pressure Effect on an Ocean-Based Humidification-Dehumidification Desalination Process." Desalination 468 (October 15, 2019): 114056. https://doi.org/10.1016/j.desal.2019.06.022.

Pressure effect on an ocean-based humidification-dehumidification desalination process

Yingchen Yang*

Department of Mechanical Engineering
University of Texas Rio Grande Valley
Brownsville·Edinburg·Harlingen, TX, USA

Abstract

A new humidification-dehumidification (HDH) desalination process is proposed and analyzed. Being ocean based, the process does not produce any brine. It is largely powered jointly by solar energy, wind energy, and various types of ocean energies in a nearly natural way. A vacuum pump is employed to drive the air circulation throughout the HDH process. It is the only unit that consumes electricity. The HDH process is analyzed under various conditions, including using a low pressure (as low as to 0.2 atm) for humidification and the ambient pressure for dehumidification, running the entire HDH process around a low pressure (as low as to 0.2 atm), and running it around the ambient pressure. The results from case studies show that applying different pressure levels to humidification and dehumidification would lead to a prohibitively high electric energy consumption of the vacuum pump. Being the most favorable operating condition, running the HDH process around the ambient pressure yields a freshwater production rate at the level of 4 to 11 l/h per HDH line, depending on the pipe sizing and weather conditions. The associated minimum electric energy consumption of the vacuum pump is at the level of 0.9 to 1.6 kWh/m^3-water.

Keywords: HDH desalination, ocean based, pressure effect, freshwater production rate, electric energy consumption.

* Email address for correspondence: yingchen.yang@utrgv.edu

1. Introduction

Scarcity of freshwater has been worsening due to population growth, industrialization, contamination of available freshwater resources, and climate change [1]. From 2012 to 2017, water crises have consistently featured among the top three most impactful global risks in the World Economic Forum's annual reports. At present, over a half of the world's population (4 billion people) lives under conditions of severe water scarcity for at least one month a year [2]. By 2050, this population could increase to 75% [3].

In contrast to the scarcity of freshwater, seawater takes about 97% of the Earth's water [4], making it an overly abundant and inexhaustible resource for freshwater production. And, currently over 40% of the global population lives within 100 km of the coast [5]. Obviously, low-cost and environment-friendly seawater desalination could effectively address the water stress issue to this large population in coastal regions worldwide.

To date, a large variety of desalination technologies, including conventional and emerging ones, have been proposed, investigated, or installed for freshwater production. In general, desalination technologies can be classified as membrane-based and thermal-based, according to the principle of operation [6]. Some technologies are particularly suited for large-scale desalination ($\geq$ 100 m^3/day, with the largest desalination plant reaching 624,000 m^3/day [7]); operating them in a small capacity makes freshwater production on a unit volume basis too expensive. Other technologies are better suited for small-scale applications (< 100 m^3/day, or even down to a level of 1 l/day [8]); their freshwater production rates are largely limited by source availabilities and/or cost constraints. Large-scale desalination can effectively augment the supply of municipal water, whereas small-scale desalination mostly meets decentralized needs for rural areas (including islands) and isolated homes [9, 10].

Most commonly used conventional large-scale desalination technologies include the membrane-based reverse osmosis and thermal-based multi-stage flash [11]. Presently, reverse osmosis has the largest installed capacity worldwide [12], and is the most energy-efficient (but not necessarily the most cost-efficient) desalination technology in market [1]. Small-scale desalination technologies,

as opposed to the large-scale ones, are very diverse. With a particular focus on thermal-based desalination using a gas (mostly air) as a carrier medium, the small-scale technologies include humidification-dehumidification (HDH) desalination [9, 10], solar stills [8], and direct freshwater extraction from ambient air [13]. HDH desalination systems are fundamentally different from solar stills and conventional distillation systems, featuring the usage of gas flows to absorb water molecules from seawater or brackish water (humidification) and transport and dump them to a freshwater collector (dehumidification).

Numerous HDH desalination systems have been explored in recent years. A common way to categorize them is based on the cycle configuration, which defines three categories: open-air open-water, open-air closed-water, and closed-air open-water [9]. Most HDH desalination systems directly utilize renewable energy (mainly solar energy) for heating to lower the cost [14, 15]. They generally operate under relatively low temperature conditions (in comparison with conventional distillation) in the humidification process, with temperatures of inlet air and/or water being raised by a few degrees Celsius to a few tens of degrees Celsius from the ambient temperature but still below the water boiling point. The naturally existing dilute solar flux (at a level of 1000 W/m^2), however, can only provide limited amount of power per unit area of an absorber to compensate the latent heat of water vaporization at a low level, largely limiting the freshwater production rates of the HDH systems. Among a large variety of solar HDH systems being explored so far, the most energy-efficient one is a multi-effect closed-air open-water system [16].

As one of the two key components—the humidifier and dehumidifier—in a typical HDH system, the humidifier can be configured in various ways employing different mechanisms, including packed bed towers, wetted-wall towers, spray towers, and bubble columns [9, 17]. Heat and mass transfer rates on the solid boundaries and/or air-water interfaces are the major concerns in design and optimization of the humidifier. Flow interaction with the internal structure of the humidifier has also been considered in some studies. For example, an earlier numerical study indicated that a high humidity level of the entrance air could adversely affect the humidifier performance under certain conditions, due to a local flow reversal that increases condensation [18]. Between humidification and dehumidification lines, heat recovery has been employed in nearly all HDH

systems. It should be noted though, that in certain HDH systems using humidifier outlet water to cool dehumidifier inlet air may increase production cost along with system productivity [19].

The carrier medium (e.g., air) is essential in HDH desalination. Either increased temperature or reduced pressure could largely enhance the capability of the medium to carry water molecules, which is in favor of humidification. The exact opposite is preferred in dehumidification. Therefore, both the temperature and pressure play a critical role in HDH desalination. A huge majority of HDH systems operates by heating for humidification and cooling for dehumidification with the pressure around the ambient pressure. In contrast, only a very few investigations have analyzed HDH systems at a largely varied pressure [20, 21].

HDH desalination systems can be either land-based (for desalination of seawater or brackish water) or ocean-based (for seawater desalination). Land-based systems permit easy construction, operation and maintenance. In fact, many solar-powered and land-based HDH desalination systems have demonstrated low cost and low-maintenance needs [14, 22]. For this reason, nearly all the HDH systems documented in the literature are land-based. In an attempt to directly use ocean energies (waves, ocean thermal, etc.) in HDH desalination, however, a very few ocean-based HDH systems have been proposed in invention disclosures [23-25].

In a much broader scope than HDH desalination, energy consumption and associated environmental impacts are critical issues all types of desalination technologies need to address. Presently, large-scale desalination (e.g., reverse osmosis, multi-stage flash, etc.) consumes a huge amount of energy in the form of thermal and electric energy derived from fossil fuels, creating a large carbon footprint [1, 10]. Under a typical desalination condition, e.g., for seawater at 35,000 ppm salt and with 50% of seawater converted to freshwater, the theoretical minimum energy consumption that is independent of the desalination method is 1.06 kWh/m^3-water [1]. Current state-of-the-art seawater reverse osmosis desalination, being the most energy-efficient in market, consumes 2.5 – 4.0 kWh/m^3-water [26]. In general, most desalination technologies include five typical stages – intake, pretreatment, pure water separation from seawater, post treatment, and brine discharge. Among these stages, intake and pretreatment together consume the second most energy next to pure water separation [26]. Therefore, enabling new desalination technologies to

eliminate the intake and pretreatment stages would greatly reduce the energy consumption and capital cost. It should be noted though, that pretreatment of feed water is needed for most desalination processes [27]. Brine is another factor worth considering. Brine is a byproduct of nearly all types of desalination processes. Direct discharge of brine to the ocean causes environmental issues [28]. Appropriate handling of brine, however, leads to added cost [29, 30].

To address the energy challenge, tremendous efforts and advancements have been made in utilizing renewable energy in desalination, either directly (without converting into electricity) or indirectly (converting into electricity first). Whenever possible, direct use is advantageous over indirect use since it can avoid employment of costly energy converters (e.g., photovoltaic panels, wind turbines, wave energy converters, etc.) and the associated waste of energy due to the limited conversion efficiencies. Direct-use renewable energy sources include solar [31, 32], geothermal [33, 34], ocean wave energy [35, 36], and ocean salinity gradient energy [37]. For HDH desalination, direct use of solar energy is very common. Direct use of ocean thermal energy (mainly for cooling in dehumidification) and ocean wave energy have also been proposed in invention disclosures [23-25]. Nonetheless, a direct and joint usage of multiple renewable energy sources to increase the freshwater production and lower the cost is yet to be demonstrated.

To address some common issues associated with the HDH desalination in general, and to gain new knowledge of pressure effect in the HDH process, an ocean-based and surface-floating HDH desalination system is proposed and discussed in the present research. The system directly uses multiple renewable energy sources to power the HDH process, with a vacuum pump to be the only unit that consumes electricity. It could work under different types of pressure conditions to achieve a desired HDH performance. The ocean deployment (by, or close to, the shoreline) enables a much simpler process with no intake and pretreatment stages and no brine production. The focus of the present work is to gain fundamental understanding by analytical means to guide the design of such an HDH system.

2. The Proposed HDH System

As schematically illustrated in Fig. 1, the proposed HDH system comprises a humidifier, a vacuum pump, a freshwater tank, pipelines, and a throttling valve. These units form a closed-air open-water system. The system essentially has two subsystems – a humidification line as indicated by dashed arrows and a dehumidification line denoted by solid arrows. The vacuum pump coordinates with the throttling valve to realize different pressure levels in the two lines. The vacuum pump also drives the air circulation throughout the entire HDH system. In the following, the working principle of the system is discussed in detail. Some key positions are numbered from 1 to 8 as shown in Fig. 1 to ease the discussion.

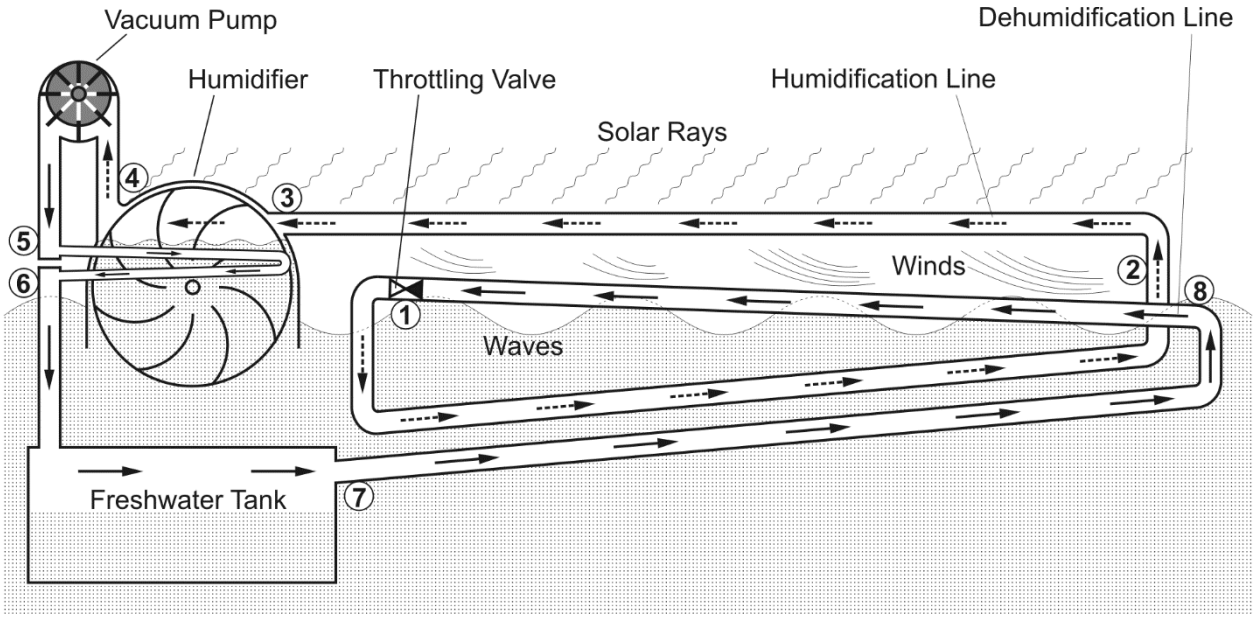

Figure 1: The proposed HDH desalination system.

Heating process: 1→2→3. The heating process of the dry airflow starts immediately after the throttling valve at position 1. Initially the dry air has a temperature below the ambient temperature by certain degrees Celsius (e.g., 10°C below). It moves along a submerged pipe segment (1→2). This pipe segment has a high thermal conductivity, so the airflow inside is gradually heated up by the surrounding seawater by means of ocean thermal energy and reaches the ambient temperature. Waves, tides and ocean currents broadly exist in the ocean and carry ocean hydrokinetic energy. Driven by that, a huge body of the seawater continuously moves irregularly in the open ocean.

Therefore, it can naturally and effectively maintain the ambient temperature around the pipe all the time. In the next step, the temperature-recovered dry air goes into an utterly above-water pipe segment (2→3) – a solar thermal heater. The heater absorbs solar energy and raises the temperature of the inside airflow by certain degrees Celsius (e.g., 30°C or more) above the ambient temperature. Note that the heater generally has a good thermal insulation capability to prevent energy loss.

Humidification process: 3→4. After the two-step heating, the warm dry air enters the humidification chamber, and grazes past wetted surfaces to gain humidity. The humidification process can be further enhanced by heating the in-chamber water by means of heat recovery (to be discussed in the following) and solar heating. The wetted surfaces are provided by a stack of partially submerged circular discs spaced out along a horizontal axle. Cloth and/or some structural patterns can be applied to the disc surfaces to increase the water carrying capability of the surfaces and enhance heat and mass transfer on the surfaces through flow interaction with the structure. The shear stress resulted on the surfaces by the grazing airflow automatically drives the stack of discs to slowly rotate about the horizontal axle and continuously bring fresh wet surfaces into contact with the airflow. Note that the humidification chamber has an open bottom, which allows free mixing of the in-chamber seawater and the surrounding seawater. Such free mixing, naturally driven by the ocean hydrokinetic energy and further enhanced by rotation of the stack of discs, maintains the salinity of the in-chamber seawater at nearly the same level with the surrounding seawater all the time. Obviously, such an HDH process has no needs for intake and pretreatment. And, it literally produces zero brine just like the natural hydrologic cycle. Also note that the water level inside the dehumidification chamber could be higher than the average ocean surface level if a vacuum pressure is created in the humidification line that includes the humidification chamber.

Settlement and pressure regulation: 4→5. Upon exiting the humidifier at position 4, the moisture-laden air enters a vertical passage to reach the vacuum pump. This vertical passage serves as a settlement chamber to allow entrained heavy impurities, if any, to fall down due to gravity and return to seawater. After the vacuum pump, the moisture-laden air is compressed to a relatively high pressure with a temperature increase due to the power input from the pump. The temperature increase can vary largely, depending on the desired pressure gain through the pump.

Cooling and dehumidification processes: 5→6→7→8→1. After position 5, the moisture-laden air moves along the dehumidification line as denoted by solid arrows in Fig. 1 and goes through three cooling phases as discussed in the following. As a result, condensation occurs with continuous heat release. The entire dehumidification line, including the tank and pipes, are made of highly thermal-conductive materials. All the pipe segments for cooling are tilted away from the horizontal direction to allow the condensed freshwater anywhere in the pipeline to eventually flow into the freshwater tank, driven by the gravity.

Cooling phase I: 5→6. As illustrated in Fig.1, a thin pipe winds through the humidification chamber right beneath the water surface. While the moisture-laden air flowing through this pipe segment is hot, the seawater in the humidification chamber is relatively cold. The heat exchange then results in initial cooling of the air and local heating of the seawater. The emphasis herein is on the seawater heating rather than the air cooling, since raising the temperature of the in-chamber seawater is much needed for humidification as addressed in the foregoing, and the hot air has more chances to be further cooled in later phases. This pipe segment is placed as close to the free surface of the in-chamber seawater as possible because the humidification chamber has an open bottom, permitting a quick mixing and exchange of the in-chamber seawater and surrounding seawater but giving the in-chamber surface seawater more time to absorb heat. Note that the presence of the pipe segment inside the humidification chamber does not interfere with rotation of the stack of discs and surface wetting. The pipes run through gaps between the circular discs only.

Cooling phase II: 6→7→8. Starting from position 6, the moisture-laden air passes through the freshwater tank and enters the next underwater pipe segment (7→8). Open ocean water moves all the time and dissipates heat quickly. Special designs can be implemented to the tank and pipe to increase the cooling surface and enhance condensation. Examples include employing a large number of pipes with small diameters, using fin structures [9] or string arrays [38], etc. At the end of this cooling phase, position 8, the temperature of the in-pipe moist air drops to the ambient temperature, and a portion of freshwater extraction is achieved.

Cooling phase III: 8→1. The moist air goes into a barely above-water pipe segment (8→1) for continuous cooling and dehumidification. This above-water pipe segment can be reached, and maintained wet on the outside, by waves. It uses evaporative cooling enhanced by winds to bring the temperature down. A shade from the above-laying solar-heating pipe segment (2→3, typically an array of pipelines) helps even more in sunny days. As a result, the temperature of the in-pipe moist air could drop by more than 10°C below the ambient temperature, allowing more freshwater extraction. The dehumidification process ends right before the throttling valve at position 1, and the cold dry air is ready to go through the valve and start the next cycle of the HDH process.

Renewable energy and heat recovery. In the HDH desalination process in Fig. 1, multiple renewable energy sources are directly used in heating for humidification, cooling for dehumidification, and mixing and transporting for maintaining the salinity and temperature levels. For example, in the humidification line 1→2→3→4, the submerged pipe segment 1→2 uses ocean thermal energy assisted by ocean hydrokinetic energy for heating, the above-water segment 2→3 uses solar energy for heating, and the humidification chamber 3→4 uses solar energy for heating and ocean hydrokinetic energy for maintaining the salinity level of the in-chamber seawater. In the dehumidification line 5→6→7→8→1, the submerged tank and pipelines 5→6→7→8 use ocean thermal energy assisted by ocean hydrokinetic energy for cooling, and the above-water pipe segment 8→1 uses wave energy and wind energy for evaporative cooling. Heat recovery makes energy utilization more efficient. By means of heat recovery, the energy rejected in cooling for dehumidification is partially used in heating for humidification. This approach is reflected between the energy-rejecting pipe segment 5→6 and the energy-absorbing seawater inside the humidifier chamber, and between the two closely placed parallel pipe segments 7→8 and 1→2 in the open ocean water.

In summary, the proposed HDH desalination system in Fig. 1 has no intake or pretreatment stage and produces zero brine. The process is largely powered by multiple renewable energy sources (i.e., solar, wind, wave, tidal, ocean current, and ocean thermal) in their natural forms (direct use) and in a combined fashion. A vacuum pump is the only device in the whole system that consumes electricity. The system has a very simple overall structure. And, renewable energy sources on the

ocean site are very abundant. Jointly considering these factors, the system demonstrates a strong potential to produce freshwater at a high rate and a low cost compared to other HDH technologies.

3. Analyses Based on Psychrometry, Thermodynamics, and Fluid Mechanics

In support of the HDH desalination approach discussed in the foregoing and to guide the engineering design of such an HDH system, some basic analyses have been performed. They are based on psychrometry, thermodynamics, and fluid mechanics.

3.1. Water Carrying Capability of Air

An online humidity calculator [39] was used to obtain some data, which reveal the water carrying capability of air in relation to the temperature and pressure. The HDH process employs dry air as a medium to absorb water vapor and form moist air. The amount of water vapor that air may contain at a specified temperature and pressure reaches the maximum at saturation, and the corresponding relative humidity (RH) is 100%. Fig. 2 shows the mixing ratio (x) of moist air, defined as the ratio of mass of water vapor (m_v, kg-water) to mass of dry air (m_a, kg-air), as a function of pressure (p) at a few fixed values of temperature (T) and at 100% RH. Focusing on individual curves, the mixing ratio increases with reduced pressure at a fixed temperature. The closer of the pressure approaches the water boiling point (towards the left of each curve), the faster the mixing ratio grows. Comparing the three representative curves, the mixing ratio goes up with increased temperature at a fixed pressure (e.g., p = 0.2 atm).

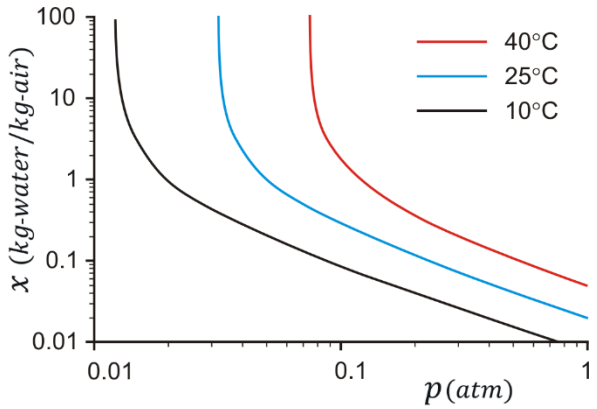

Figure 2: Variation of mixing ratio x with pressure p at three specified values of temperature T.

3.2. A Thermodynamic Model for Temperature and Energy Analyses

In the examined ranges of pressure and temperature in the present study, the moist air as well as its constituent air and vapor components all obey the ideal gas law with sufficient accuracy, and the thermodynamic properties of the moist air can be obtained by means of linear superposition of the corresponding air and vapor properties [40, 41]. The ideal gas properties (e.g., specific enthalpy *h* and entropy function s^o) of dry air and water vapor are available in Tables A-22 and A-23 of reference [42]. Eqs. 1 – 6 provides an approach to determine needed properties of the moist air, which are of particular interest in the present study. In Eqs. 1 – 6, symbols with subscripts *a* and *v* denotes corresponding properties of air and water vapor, respectively (e.g., partial pressures p_a and p_v, entropy functions s_a^o and s_v^o, specific entropies s_a and s_v, enthalpies h_a and h_v, and gas constants R_a and R_v). Symbols with no subscripts represents corresponding properties of the moist air as a mixture (e.g., total pressure *p*, specific entropy *s*, and specific enthalpy *h*). To calculate *h* and *s* of the moist air at given *T*, *p* and RH, the mixing ratio *x* needs to be determined first [39], followed by p_v and p_a using Eqs. 1 & 2 [40], s_a and s_v using Eqs. 3 & 4 [42], and then *h* and *s* using Eqs. 5 & 6 [40]. Note that the specific enthalpy *h* and specific entropy *s* of the moist air are based on unit mass of dry air.

$$p_v = xp/(0.622 + x) \tag{1}$$

$$p_a = p - p_v \tag{2}$$

$$s_a = s_a^o - R_a ln\frac{p_a}{p_{ref,a}} \tag{3}$$

$$s_v = s_v^o - R_v ln\frac{p_v}{p_{ref,v}} \tag{4}$$

$$h = h_a + xh_v \tag{5}$$

$$s = s_a + xs_v \tag{6}$$

Upon the availability of these thermodynamic properties, the proposed HDH desalination system of Fig. 1 can be analyzed from thermodynamics perspective. Particularly, the temperature gain of the circulating moist air through solar thermal heating, the temperature drop of it due to humidity gain in humidification, and the minimum electric energy consumption of the vacuum pump per unit volume of freshwater production can be quantified. For easy discussion, the position numbers

in the HDH system of Fig. 1 are used as subscripts to denote properties/parameters of the moist airflow at the corresponding positions. For example, position 3 indicates the inlet of the humidifier. At this position, the temperature (T), pressure (p), mixing ratio (x), specific enthalpy (h), specific entropy (s), and the average airflow velocity (V) are denoted as T_3, p_3, x_3, h_3, s_3, and V_3 accordingly.

Solar thermal heating 2→3 in Fig. 1 leads to a temperature gain $T_3 - T_2$. By selecting the pipe segment 2→3 as a control volume and apply the first law of thermodynamics, it gives

$$h_3 = h_2 + \frac{\dot{Q}}{\dot{m}_1}, \tag{7}$$

where $\dot{m}_1$ is the mass flow rate of the moist air at position 1 ($\dot{m}_1 = \dot{m}_2 = \dot{m}_3$), and $\dot{Q}$ is the heat transfer rate due to the solar irradiance. $\dot{Q}$ is obtained by conservatively assuming a 50% conversion efficiency of the 1-kW/m^2 solar power intensity, which is in comparison with 70-90% efficiencies of industrial solar thermal heaters and accounts for humidity effect over the ocean surface. For moist air as an ideal gas at a specified x, h is a function of T only (implicitly by means of Eq. 5 and the thermodynamic property tables [42]). In this heating phase there is no humidity gain or loss, $x_2 = x_3$. Therefore, a given T_2 is associated with a known h_2, which leads to determination of h_3 using Eq. 7. Inversely, the resulted h_3 defines T_3.

In the humidification process 3→4, the grazing airflow loses energy to the surface water (mainly on the roller discs), leading to a temperature drop ($T_4 < T_3$) of the airflow and a humidity gain ($x_4 > x_3$) through evaporation. Select the humidifier as a control volume, and assume a 100% energy transfer from the entering airflow at T_3 to the surface water that evaporates at T_4. Other means of energy gain (e.g., solar thermal heating on the humidifier) or loss are neglected. Note that T_4 should be still above the ambient temperature. Heat recovery as discussed in Section 2 can help bring the surface water temperature from the ambient temperature to T_4 through careful design. Applying the first law of thermodynamics to the control volume (excluding the heat recovery part but assuming the surface water at T_4) gives

$$(1 + x_4)h_4 = (1 + x_3)h_3 + (x_4 - x_3)h_w, \tag{8}$$

where h_w is the specific enthalpy of liquid water at T_4. In this equation, x_4, h_w and h_4 all depend on T_4. The equation can be solved through iteration by using thermodynamic property tables [42]

in conjunction with the online humidity calculator [39]. Then with known h_4, T_4 can be found from the property tables.

The vacuum pump 4→5 in the HDH desalination system of Fig. 1 is the only unit that consumes electricity. Other than that, the entire HDH process is directly powered by multiple renewable energy sources in a nearly natural way with very low cost. Choose the vacuum pump in steady-state operation as a control volume. Assume that after a perfect humidification, the moist air reaches a desired humidity level of 100% RH at position 4 with T_4, p_4 and x_4. The moist air then goes through the vacuum pump and the outlet pressure at position 5 rises to a desired level p_5. In this thermodynamic process, no condensation occurs; the pressure increase through the vacuum pump is accompanied by a temperature increase due to the power input. Therefore, the mixing ratio remains unchanged from the inlet to the outlet, $x_4 = x_5$. Now with known T_4, p_4 and p_5, the minimum power input can be achieved by assuming an isentropic process, $s_4 = s_5$. Then based on the first law of thermodynamics, the minimum electric power input ($\dot{W}$) per mass flow rate of dry air ($\dot{m}_a$) is equal to the enthalpy increase,

$$\dot{W}/\dot{m}_a = h_5 - h_4. \tag{9}$$

In this equation, h_4 can be determined using T_4, p_4 and x_4, whereas h_5 depends on p_5, s_5 ($= s_4$) and x_5 ($= x_4$).

After the vacuum pump the moist air goes through a series of cooling phases for dehumidification until it reaches the inlet of the throttling valve at position 1. The mixing ratio x_1 at this position can be determined with given T_1, p_1 and 100% RH using the same online humidity calculator as mentioned before. Then based on Eq. 9, the minimum electric energy consumption per unit volume of freshwater production in liquid phase can be determined as

$$W_w = \frac{998(h_5 - h_4)}{3600(x_4 - x_1)}, \tag{10}$$

where h_4 and h_5 are in kJ/kg, and W_w is in kWh/m^3-water. Additionally, with known x_1, x_4 and $\dot{m}_1$, the freshwater production rate $\dot{m}_w$ can be calculated using

$$\dot{m}_w = \frac{3600(x_4 - x_1)\dot{m}_1}{0.998(1 + x_1)}, \tag{11}$$

where $\dot{m}_1$ is in kg/s, and $\dot{m}_w$ is in l/h of liquid water.

3.3. A Fluid Mechanics Model for Pressure Loss Estimate

As evident in Fig. 2, a low pressure is in favor of humidification and a high pressure in dehumidification. To keep air circulation in the HDH process as illustrated in Fig. 1, a minimum pressure gain from the inlet 4 to the outlet 5 of the vacuum pump is needed. This gain is used to overcome the pressure loss in the humidification and dehumidification lines as well as on the rolling discs of the humidifier. If the humidification line and dehumidification line need to be set at different pressure levels, the pump's pressure gain should be greater than the minimum one; the additional pressure gain is to be applied on the throttling valve to achieve the expected pressure levels.

To quantify the pressure loss in the humidification and dehumidification lines in Fig. 1, the viscosity μ (in Pa·s) and density ρ (in kg/m^3) of the humid air at a specified temperature T (in K), pressure p (in Pa), and mixing ratio x can be determined using [43]:

$$\mu = \frac{\mu_a}{1 + 0.3519\left[1 + 0.8881\left(\frac{\mu_a}{\mu_v}\right)^{0.5}\right]^2 \cdot x} + \frac{\mu_v}{1 + 0.1727\left[1 + 1.1260\left(\frac{\mu_v}{\mu_a}\right)^{0.5}\right]^2 / x}, \quad (12)$$

$$\mu_a \cdot 10^6 = 0.40401 + 0.074582T - 5.7171 \cdot 10^{-5}T^2 + 2.9928 \cdot 10^{-8}T^3 - 6.2524 \cdot 10^{-12}T^4, \quad (13)$$

$$\mu_v \cdot 10^6 = \frac{\sqrt{\frac{T}{647.27}}}{0.0181583 + 0.0177624\left(\frac{647.27}{T}\right) + 0.0105287\left(\frac{647.27}{T}\right)^2 - 0.0036744\left(\frac{647.27}{T}\right)^3}, \quad (14)$$

$$\rho = \frac{1 + x}{461.56 \cdot (0.62198 + x)} \cdot \frac{p}{T}. \quad (15)$$

Upon determination of μ and ρ, the pressure loss Δp of a fully developed turbulent internal flow of moist air along a circular pipe at a constant temperature T with no occurrence of condensation can be calculated using the following equations [44]:

$$Re = \frac{\rho V D}{\mu}, \quad (16)$$

$$\frac{1}{f^{1/2}} \approx -1.8 log\left[\frac{6.9}{Re} + \left(\frac{\varepsilon/D}{3.7}\right)^{1.11}\right], \quad (17)$$

$$\Delta p = \frac{f L \rho V^2}{2D}. \tag{18}$$

In these equations, Re is the Reynolds number, V the average flow velocity of moist air, D the pipe inner diameter, ε the pipe inner surface roughness, L the pipe length, and f the Darcy friction factor. Eq. 17 applies to turbulent pipe flow, which occurs when $Re \geq 4000$ [44].

The pipe flow in the proposed HDH system in Fig. 1 has varied temperature T and mixing ratio x, which complicate the pressure loss calculation. Focusing on the airflow along the pipeline between the freshwater tank (position 7) and the throttling valve (position 1), the moist air undergoes two cooling phases – ocean thermal cooling 7→8 and evaporative cooling 8→1. Condensation occurs in these two phases at 100% RH, and the mixing ratio decreases with decreasing temperature. In contrast, the airflow along the pipeline between the throttling valve (position 1) and the humidifier (position 3) experiences two heating phases – ocean thermal heating 1→2, and solar thermal heating 2→3. The air in these heating phases has no gain or loss of water. Hence, the relative humidity decreases with increasing temperature, but the mixing ratio remains constant.

To apply Eqs. 12 – 18 for an approximate estimate of a total pressure loss along a pipe length L, and to deal with the variations in temperature, mixing ratio and other parameters, the full pipe length L is divided into a large number of differential length dL for differential pressure dp first. Then the total pressure loss is obtained through numerical integration. In doing so, the temperature distribution along the pipe needs to be known. Additionally, the local velocity V at any position along the pipe can be determined using

$$V = \frac{1 + x}{1 + x_1} \frac{\rho_1}{\rho} V_1. \tag{19}$$

This equation is derived from mass conservation. In applying Eqs. 12 – 19 to determine the total pressure loss, the pressure drop due to the presence of the throttling valve is excluded. Minor losses on the pipe fittings (e.g., elbows/bents, etc.) are also ignored.

4. Case Studies

Consider an HDH system as illustrated in Fig. 1 in a utility scale. A pipe of inner diameter D = 0.15 m and length L = 100 m is employed along the airflow direction 7→8→1→2→3. In practice, arrays of such pipes are to be applied in parallel to gain a high production rate of freshwater. Assume that the full length L is evenly divided into four segments: 7→8 for ocean thermal cooling, 8→1 for evaporative cooling, 1→2 for ocean thermal heating, and 2→3 for solar thermal heating. In this case study, two scenarios are analyzed – without throttling and with throttling.

4.1. An HDH System without Throttling

In this scenario, the throttling valve at position 1 is removed from the HDH system in Fig. 1. Some temperature conditions are given, assumed (based on some educated guesses, or for the easiness of analysis), and/or derived. They are discussed as follows. (1) At positions 2 and 8, the temperature recovers to a specified ambient temperature (e.g., $T_2 = T_8 =$ 10°C, 20°C, 30°C, or 40°C). (2) A 10°C temperature drop is assumed through evaporative cooling (8→1), $T_1 = T_8 -$ 10°C; the real temperature drop could be largely affected by the wind condition. (3) T_3 at the end of solar thermal heating (2→3) is obtained using Eq. 7 implicitly. (4) T_4 at the end of the humidification process (3→4) is determined using Eq. 8 implicitly. (5) T_5 at the outlet of the vacuum pump is found with known T_4, p_4 & p_5 and by assuming an isentropic process through the vacuum pump (for the minimum electric power consumption). (6) T_7 is set by assuming $T_5 - T_7 = (T_5 - T_8)/3$. (7) Linear temperature distributions are assumed in the pipe segments 7→8, 8→1, 1→2, and 2→3.

In addition to the temperature information, the pressure p_1 and the average velocity V_1 are also set to be the controlling parameters in this case study. The pressures p_2, p_3, p_7, and p_8 then become determinable using Eqs. 12 – 19 together with the online humidity calculator [39]. The pressures p_4 and p_5 can be largely affected by the detailed humidification and heat recovery mechanisms. Their levels are roughly set by assuming $p_3 - p_4 \approx p_1 - p_3$ and $p_5 - p_7 \approx p_7 - p_1$, based on an educated guess. This assumption leads to $\Delta p_{vacuum} = 2\Delta p_{7-3}$, where Δp_{vacuum} is the pressure gain through the vacuum pump, $\Delta p_{vacuum} = p_5 - p_4$, and $\Delta p_{7-3} = p_7 - p_3$. Then with known

p_4, p_5 and other information as needed, the minimum electric energy consumption of the vacuum pump can be quantified using Eq. 10.

Using the above conditions and approaches, the first computation run was conducted at $T_1 = 10$°C, $p_1 = 1$ atm, and $V_1 = 2.5$ m/s. The results of some parameters at the positions numbered in Fig. 1 are summarized in Table 1. Additionally, the pressure drop between positions 7 and 3 is $\Delta p_{7-3} = 6.56\times10^{-4}$ atm, the freshwater production rate is $\dot{m}_w = 5.24\ l$/h, and the vacuum pump's minimum electric energy consumption is $W_w = 1.26$ kWh/m^3-water. The computation conditions and results are further interpreted as follows.

Table 1: Computation results at $p_1 = 1$ atm, $T_1 = 10$°C, and $V_1 = 2.5$ m/s.

Position	p (atm)	T (°C)	x	V (m/s)	Re	h (kJ/kg)	s (kJ/kg·K)
1	1.00000	10.0	0.0076	2.50	26626	287.3	1.74
2	0.99984	20.0	0.0076	2.58	25911	297.4	1.78
3	0.99967	53.6	0.0076	2.88	23856	331.7	1.89
4	0.99934	33.9	0.0344	×	×	326.8	2.15
5	1.00066	34.0	0.0344	×	×	326.9	2.15
7	1.00033	29.4	0.0262	2.75	26107	317.4	2.04
8	1.00016	20.0	0.0147	2.62	26233	301.3	1.86

The temperature $T_1 = 10$°C is associated with an ambient temperature of 20°C (T_2 and T_8). The pressure $p_1 = 1$ atm and the pressure drop $\Delta p_{7-3} = 6.56\times10^{-4}$ atm jointly define the pressure level throughout the HDH system to be at the ambient pressure with very little changes. The velocity $V_1 = 2.5$ m/s is equivalent to a light breeze according to the Beaufort wind scale, which is low enough to permit easy occurrence of condensation. The Reynolds number $Re_1 = 26626$ ensures a fully turbulent pipe flow ($Re > 4000$) that is in favor of quick heat exchanging between the in-pipe moist air and the surrounding environment. The freshwater production rate per HDH line, $\dot{m}_w = 5.24\ l$/h, is very promising compared to other state-of-the-art HDH desalination processes [10]. Most importantly, the minimum electric energy consumption $W_w = 1.26$ kWh/m^3-water is

very close to the theoretical minimum energy consumption of 1.06 kWh/m^3-water [1], and is much lower than the state-of-the-art level of 2.5 – 4.0 kWh/m^3-water [26]. Of course, such a low energy consumption level of the present approach is achieved by counting the pump's minimum electric energy consumption only, assuming that the rest of the system is directly and sufficiently powered by all kinds of renewable energy sources at a very low cost as discussed in the forgoing.

To further reflect an overall HDH cycle (1→2→3→4→5→7→8→1) of the moist air in this first computation run, a $T-s$ diagram is presented in Fig. 3. A linear connection between any two adjacent data points is made as an approximation, just for the illustration purpose.

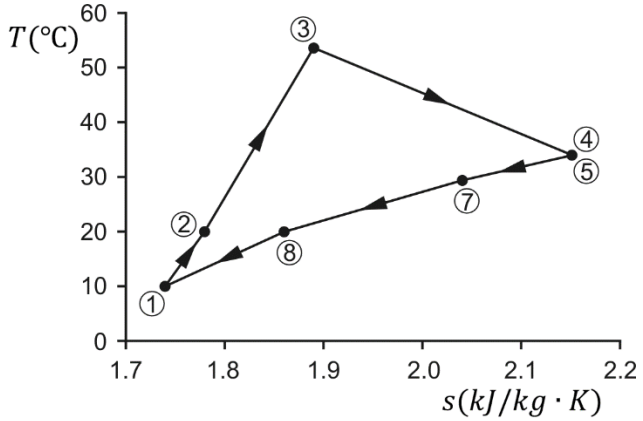

Figure 3: T – s diagram of an HDH cycle at $p_1 = 1$ atm, $T_1 = 10$°C, and $V_1 = 2.5$ m/s.

Based on the first computation run discussed in the foregoing, more runs were conducted at a fixed temperature $T_1 = 10$°C, a fixed pressure drop $\Delta p_{7-3} = 6.56\times10^{-4}$ atm, and a varied pressure p_1 in the range of 0.2 – 1 atm (in vacuum conditions). Unlike the first run where V_1 is given and Δp_{7-3} is derived, now V_1 becomes derived and Δp_{7-3} is given. The computation results are summarized in Table 2. They are also graphically presented in Fig. 4; each plot reflects a trend of a parameter with varied p_1. Note that the pressure gain created by the vacuum pump, Δp_{vacuum}, is twice the pressure drop Δp_{7-3} (as assumed earlier): $\Delta p_{vacuum} = 2\Delta p_{7-3} = 1.31 \times 10^{-3}$ at$m$. Therefore, the data in Table 2 and Fig. 4 reflect the system performance at a fixed pressure gain of the vacuum pump. Also note that this pressure gain is about two to three orders lower than the values of p_1 examined. Hence p_1 very closely represents the actual pressure level everywhere in the system.

Table 2: Computation results at $T_1 = 10$°C and $\Delta p_{7-3} = 6.56\times10^{-4}$ atm under varied p_1.

p_1 (atm)	T_3 (°C)	T_4 (°C)	T_5 (°C)	Re_1	$\dot{m}_1$ (kg/s)	$\dot{m}_w$ (l/h)	W_w (kWh/m^3)
1.0	53.6	33.9	34.0	26626	0.0548	5.24	1.26
0.8	58.1	33.6	33.8	23427	0.0482	5.71	1.30
0.6	64.8	32.9	33.1	19845	0.0407	6.24	1.33
0.4	76.2	31.4	31.7	15684	0.0320	6.83	1.49
0.2	102.6	27.7	28.3	10445	0.0210	7.31	1.94

It is evident in Fig. 4 that, the lower the pressure p_1, the higher the freshwater production rate $\dot{m}_w$ (Fig. 4b). Especially, this increased $\dot{m}_w$ (with lowered p_1) is achieved on a decreased mass flow rate $\dot{m}_1$ of the moist air (Fig. 4c). It is noteworthy though, that the increase of $\dot{m}_w$ is very limited in comparison with the significant decrease of p_1. It is more disappointing that, the lowered pressure p_1 results in an increased minimum electric energy consumption W_w (Fig. 4a). The lower the pressure p_1 becomes, the faster W_w grows. Therefore, it is economically disadvantageous to achieve an increased freshwater production rate by operating the HDH system around a vacuum pressure rather than around the ambient pressure, not to mention the complexity and additional cost on maintaining such a vacuum pressure in routine operation.

In the examined range of p_1 in Fig. 4, the Reynolds number Re_1 indicates a turbulent pipe flow condition in all the computation runs (Fig. 4d). At lowered p_1, solar thermal heating leads to climbed T_3 (Fig. 4e) due to reduced $\dot{m}_1$ (Fig. 4c). After humidification, however, T_4 shows a declined trend with lowered p_1 (Fig. 4f). This trend is mainly resulted by an enhanced evaporation of the liquid water due to the reduced pressure.

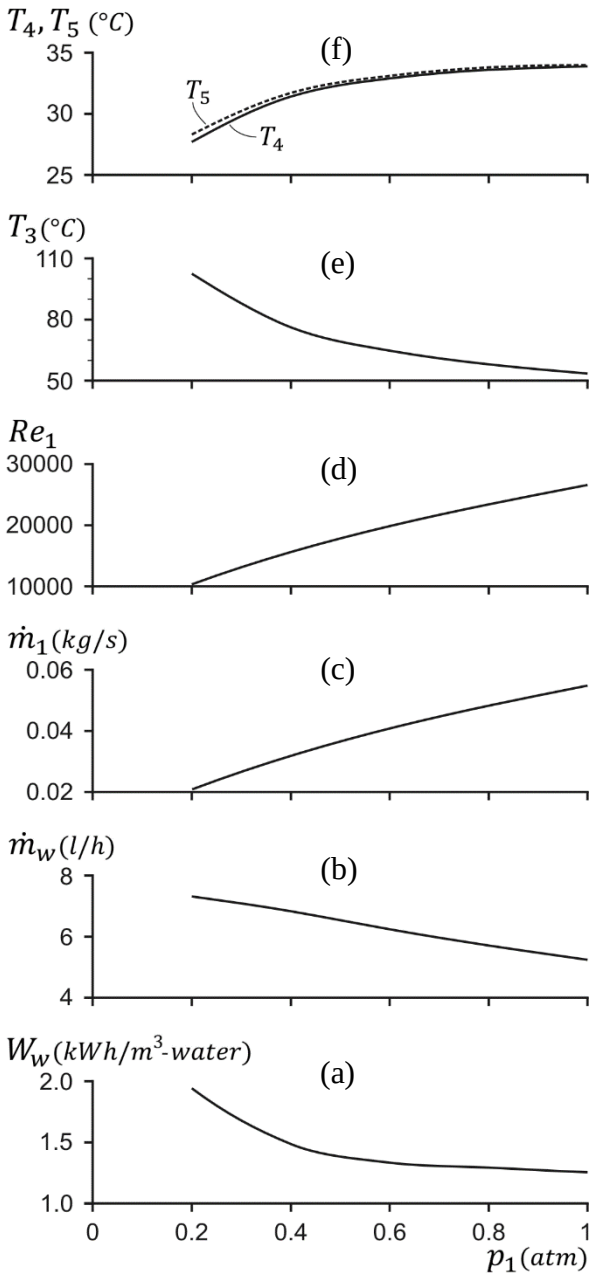

Figure 4: Graphical presentation of the results in Table 2. (a) W_w versus p_1. (b) $\dot{m}_w$ versus p_1. (c) $\dot{m}_1$ versus p_1. (d) Re_1 versus p_1. (e) T_3 versus p_1. (f) T_4 & T_5 versus p_1.

With a preferred operation condition given to $p_1 = 1$ atm, and by maintaining the same pressure drop $\Delta p_{7-3} = 6.56\times10^{-4}$ atm as before, further computation runs were conducted at varied T_1 in the range of 0 – 30°C. The results are provided in Table 3. Among the parameters listed in Table 3, W_w and $\dot{m}_w$ are plotted against T_2 in Fig. 5. Note that T_2 ($= T_1 + 10$°C) also represents the

ambient temperature. Therefore, Table 3 and Fig. 5 show the effect of the ambient temperature on the system performance.

Table 3: Computation results at $p_1 = 1$ atm and $\Delta p_{7-3} = 6.56\times10^{-4}$ atm under varied T_1.

T_1 (°C)	T_2 (°C)	T_3 (°C)	T_4 (°C)	T_5 (°C)	Re_1	$\dot{m}_1$ (kg/s)	$\dot{m}_w$ (l/h)	W_w (kWh/m^3)
30	40	74.1	45.6	45.7	24281	0.0520	7.33	0.94
20	30	64.0	39.7	39.9	25384	0.0534	6.36	1.07
10	20	53.6	33.9	34.0	26626	0.0548	5.24	1.26
0	10	43.0	27.9	28.0	28014	0.0562	4.09	1.62

In the examined range of the ambient temperature 10°C ≤ T_2 ≤ 40°C, the lower and upper ends represent ocean surface conditions on a chilly day and a hot day, respectively. As show in Table 3 and Fig. 5, with increase of the ambient temperature from 10°C to 40°C, the freshwater production rate $\dot{m}_w$ increased from 4.09 to 7.33 l/h, and the vacuum pump's minimum electric energy consumption W_w reduced from 1.62 to 0.94 kWh/m^3-water. Undoubtedly, a hot weather is in favor of the HDH desalination over a chilly weather. Still, in the entire temperature range being examined, both $\dot{m}_w$ and W_w demonstrate a very promising system performance.

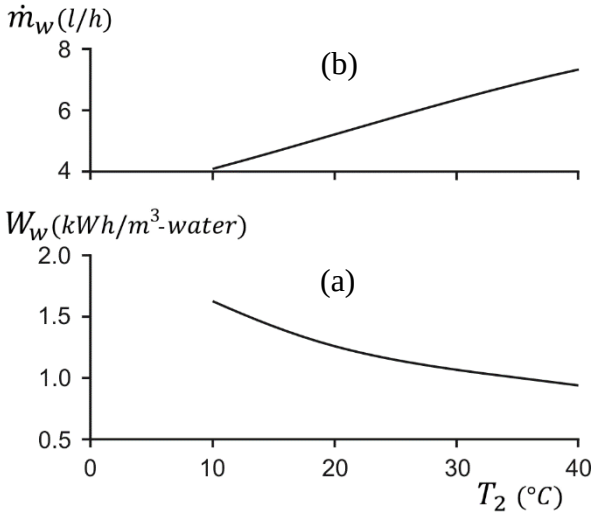

Figure 5: Graphical presentation of partial results in Table 3. (a) W_w versus T_2. (b) $\dot{m}_w$ versus T_2.

From a practical point of view, arrays of HDH lines instead of just a single one as illustrated in Fig. 1 can be employed in building a desalination plant for a high freshwater production rate. The single line freshwater production rate can also be greatly enhanced through parametric optimization. For example, by doubling the pipe diameter D from 0.15 m to 0.3 m and maintaining the average air velocity V_1 = 2.5 m/s and all the other conditions the same as before, at a comfortable ambient temperature $T_2 = 20$°C and an in-pipe pressure p_1 = 1 atm, a single line HDH system can produce freshwater at a rate of $\dot{m}_w = 11.12$ l/h with the minimum electric energy consumption of the vacuum pump to be $W_w = 0.96$ kWh/m^3-water. The results are in comparison with $\dot{m}_w = 5.24$ l/h and $W_w = 1.26$ kWh/m^3-water at $D = 0.15$ m. Of course, such results are based on an assumption that the renewable energy sources are sufficient enough to provide appropriate heating and cooling as needed.

4.2. An HDH System with Throttling

Focus on the pipe diameter $D = 0.15$ m as before. In this new scenario, the throttling valve in Fig. 1 is employed to generate a preset pressure drop $\Delta p_{throttle}$ between its inlet (namely position 1) and outlet (namely position 1′). Such a pressure drop will separate the pressure levels between the humidification line 1′→2→3→4 and the dehumidification line 5→6→7→8→1, hoping to achieve a better system performance than without throttling.

For ideal gas going through a throttling process, there is no temperature change [42]. Since the moist air is assumed to be ideal gas in the present study, the temperature throughout the throttling valve would remain the same and is denoted as T_1 as before. The other temperature conditions in this scenario are exactly the same as that in the earlier scenario. On the pressure in this scenario, p_1 and $p_{1'}$ are for the inlet (position 1) and outlet (position 1′) pressure levels of the throttling valve, $p_1 - p_{1'} = \Delta p_{throttle}$. Other pressure conditions are the same as before and are summarize herein: $p_3 - p_4 \approx p_{1'} - p_3$, $p_5 - p_7 \approx p_7 - p_1$. Based on these pressure specifications, the vacuum pump needs to create a pressure gain $\Delta p_{vacuum} = p_5 - p_4 = 2(p_7 - p_1) + \Delta p_{throttle} + 2(p_{1'} - p_3)$, where $p_7 - p_1$ and $p_{1'} - p_3$ are computed and $\Delta p_{throttle}$ is preset.

By maintaining $(p_7 - p_1) + (p_{1'} - p_3) = 6.56\times10^{-4}$ atm as before, the system performance at fixed $p_1 = 1$ atm and $T_1 = 10$°C and varied $\Delta p_{throttle}$ is presented in Fig. 6. It is evident that, with increase of $\Delta p_{throttle}$ from 0 to 0.1 atm, the freshwater production rate $\dot{m}_w$ increases by very little (Fig. 5b). In contrast, the pump's minimum electric energy consumption W_w increases almost linearly (Fig. 5a).

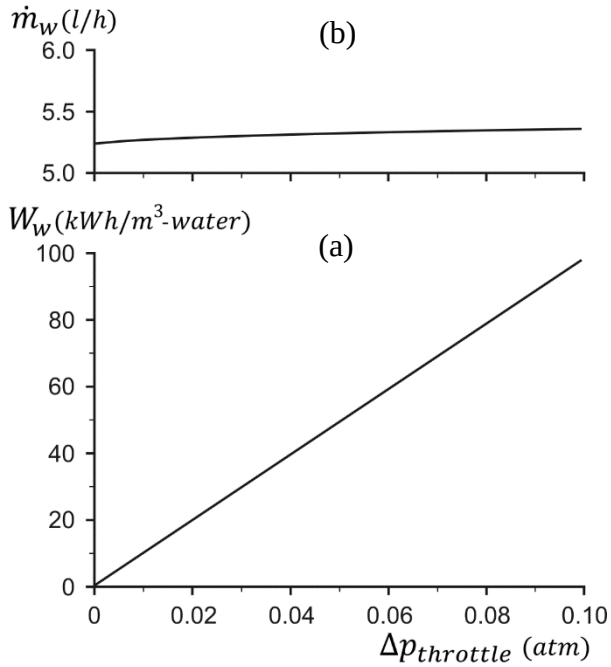

Figure 6: Computation results at fixed $T_1 = 10$°C, $p_1 = 1$ atm, $(p_7 - p_1) + (p_{1'} - p_3) = 6.56\times10^{-4}$ atm and varied $\Delta p_{throttle}$. (a) W_w versus $\Delta p_{throttle}$. (b) $\dot{m}_w$ versus $\Delta p_{throttle}$.

In a much larger range $0.1 < \Delta p_{throttle} < 1$ atm, the pressure drop $(p_7 - p_1) + (p_{1'} - p_3) = 6.56\times10^{-4}$ atm becomes negligibly small, resulting in $\Delta p_{throttle} \approx \Delta p_{vacuum}$. Then with a particular focus on the vacuum pump alone, the pump's minimum electric energy consumption W_w can be simply determined using Eq. 10 with a given T_4 at the inlet, p_5 at the outlet, and the pressure gain Δp_{vacuum}. Note that at the pump's inlet the pressure p_4 can be determined using $p_4 = p_5 - \Delta p_{vacuum}$. Fig. 7 shows the variation of W_w with Δp_{vacuum} in the range $0 < \Delta p_{vacuum} < 1$ atm at a fixed $p_5 = 1$ atm and three specified values of T_4. The three temperature values $T_4 = 28$°C, 34°C and 40°C are associated with $T_2 = 10$°C, 20°C and 30°C in the earlier scenario without throttling. As evident in Fig. 7, there is a peak of W_w versus Δp_{vacuum} for each specified T_4. The peaks occur in a narrow range $0.63 < \Delta p_{vacuum} < 0.67$. For a further increased

Δp_{vacuum} beyond the peak points (leading to a further reduced $p_4 = 1 - \Delta p_{vacuum}$), W_w goes down until a boiling pressure of p_4 is reached. Taking a global view of Fig. 7, however, it is obvious that W_w is generally one to two orders higher than that of the state-of-the-art technologies (i.e., 2.5 – 4.0 kWh/m^3-water [26]) in nearly the entire range $0 < \Delta p_{vacuum} < 1$ atm except when Δp_{vacuum} becomes very low (e.g. $\Delta p_{vacuum} = 2(p_7 - p_1) + 2(p_{1'} - p_3) = 1.31\times10^{-3}$ atm).

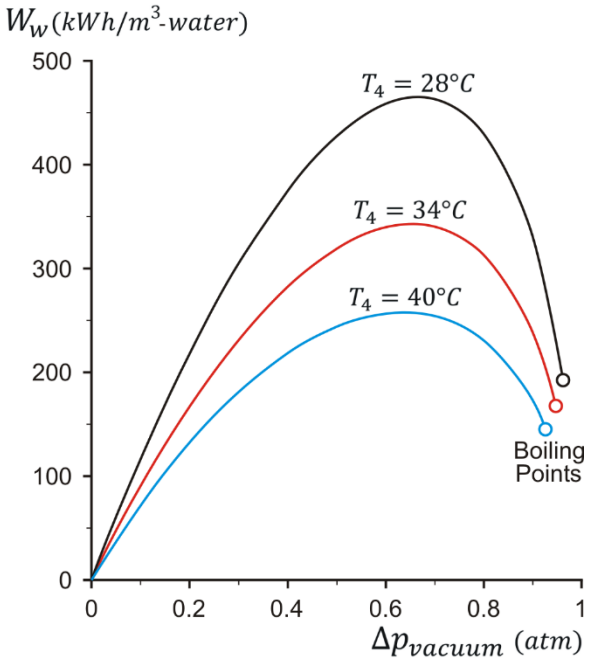

Figure 7: Variation of the vacuum pump's minimum electric energy consumption W_w with its pressure gain Δp_{vacuum} at a fixed outlet pressure $p_5 = 1$ atm and three specified inlet temperature $T_4 = 28$°C, 34°C and 40°C.

Taken Fig. 6a and Fig. 7 together and noting the relation $\Delta p_{vacuum} \approx \Delta p_{throttle}$, it becomes very clear that applying a throttling valve to separate the pressure levels between the humidification line 1′→2→3→4 and the dehumidification line 5→6→7→8→1 of Fig. 1 is economically prohibitive. Therefore, in a practical design of the HDH system in Fig. 1, the throttling valve should be removed.

5. Conclusions

An ocean based HDH desalination process is proposed. It enables a closed-air open-water system that does not produce any brine. The process is largely powered by various renewable energy sources in a nearly natural way, with a vacuum pump to be the only unit that consumes electricity. The vacuum pump is used to drive the air circulation in the HDH process. Analytical models based on psychrometry, thermodynamics, and fluid mechanics have been developed to characterize the HDH system performance. The following conclusions are drawn from case studies:

(1) Employing a throttling valve to create a vacuum pressure level in the humidification line and maintain an ambient pressure level in the dehumidification line is disadvantageous to the HDH desalination. The pump's minimum electric energy consumption per unit volume of freshwater production could be one to two orders higher than the total energy consumption per unit volume of freshwater production of the state-of-the-art desalination technologies.

(2) Making the air circulating through both the humidification and dehumidification lines at nearly the same vacuum pressure level without throttling leads to an increased freshwater production rate in comparison with running the air around the ambient pressure level. But the increase is very limited (about 40% increase by dropping the line pressure from 1 atm to 0.2 atm), and is based on an increase of the pump's minimum electric energy consumption per unit volume of the freshwater production (about 55% increase).

(3) Running the circulating air through the entire HDH system around the ambient pressure without throttling (but with some pressure loss) is the most practical and economically viable way of using the proposed HDH process for seawater desalination. The yielded freshwater production rate could be at the level of 4 to 11 l/h per HDH line, depending on the pipe sizing and weather conditions. The associated minimum electric energy consumption of the vacuum pump is at the level of 0.9 to 1.6 kWh/m^3-water.

References

1. M. Elimelech, W.A. Phillip, The future of seawater desalination: energy, technology, and the environment, Science 333 (2011) 712-717.
2. M.M. Mekonnen, A.Y. Hoekstra, Four billion people facing severe water scarcity, Sci. Adv. 2 (2016) 1–6.
3. UN-Water, Nature-based solution for water, The United Nations World Water Development Report 2018, 2018, Paris, UNESCO.
4. I. Shiklomanov, "World freshwater resources", in P.H. Gleick (editor), 1993, Water in Crisis: A Guide to the World's Freshwater Resources, Oxford University Press, New York.
5. S. Mustafa, R. Shapawi, Aquaculture Ecosystems: Adaptability and Sustainability, 1st ed., Wiley-Blackwell, 2015.
6. A. Subramani, J.G. Jacangelo, Emerging desalination technologies for water treatment – a critical review, Water Research 75 (2015) 164-187.
7. M. Kurihara, H. Takeuchi, SWRO-PRO system in Mega-ton water system for energy reduction and low environmental impact, Water 10 (2018) 48, doi:10.3390/w10010048.
8. D.D.W.Rufuss, S. Iniyan, L. Suganthi, P.A. Davies, Solar stills: A comprehensive review of designs, performance and material advances, Renewable and Sustainable Energy Review 63 (2016) 464-496.
9. A.E. Kabeel, M.H. Hamed, Z.M. Omara, S.W. Sharshir, Water Desalination Using a Humidification-Dehumidification Technique—A Detailed Review, Natural Resources, 4 (2013) 286-305.
10. A. Giwa, N. Akther, A.A. Housani, S. Haris, S.W. Hasan, Recent advances in humidification dehumidification (HDH) desalination processes: Improved designs and productivity, Renew. Sust. Energ. Rev. 57 (2016) 929-944.
11. D.S. Likhachev, F. Li, Large-scale water desalination methods: a review and new perspectives, Desalin. Water Treat. 51 (2013) 2836-49.
12. G. Amy, N. Ghaffour, Z. Li, L. Francis, R.V. Linares, T. Missimer, S. Lattemann, Membrane-based seawater desalination: Present and future prospects, Desalination 401 (2017) 16-21.
13. F. Fathieh, M.J. Kalmutzki, E.A. Kapustin, P.J. Waller, J. Yang, O.M. Yaghi, Practical water production from desert air, Sci. Adv. 4 (2018) eaat3198.

14. S. Al-Hallaj, S. Parekh, M.M. Farid, J.R. Selman, Solar desalination with humidification-dehumidification cycle: review of economics, Desalination 195 (2006) 169–86.
15. W. Abdelmoez, M.S. Mahmoud, T.E Farrag, Water desalination using humidification /dehumidification (HDH) technique powered by solar energy: a detailed review, Desalin. Water Treat. 52 (2013) 4622–40.
16. G.P. Narayan, M.H. Sharqawy, E.K. Summers,J.H. Lienhard, S.M. Zubair, M.A. Antar, The potential of solar-driven humidification-dehumidification desalination for small-scale decentralized water production, Renew. Sust. Energ. Rev. 14 (2010) 1187–201.
17. K. Srithar, T. Rajaseenivasan, Recent freshwater augmentation techniques in solar still and HDH desalination – A review, Renewable and Sustainable Energy Reviews 82 (2018) 629–44.
18. M.A. Kassim, B. Benhamou, S. Harmand, Effect of air humidity at the entrance on heat and mass transfers in a humidifier intended for a desalination system, Appl. Therm. Eng. 31 (2011) 1906–14.
19. M. Zamen, M. Amidpour, S.M. Soufari, Cost optimization of a solar humidification–dehumidification desalination unit using mathematical programming, Desalination 239 (2009) 92–9.
20. O.K. Siddiqui, M.H. Sharqawy, M.A. Antar, S.M. Zubair, Performance evaluation of variable pressure humidification-dehumidification systems, Desalination 409 (2017) 171-182.
21. Z. Rahimi-Ahar, M.S. Hatamipour, Y. Ghalavand, Experimental investigation of a solar vacuum humidification-dehumidification (VHDH) desalination system, Desalination, 437 (2018) 73-80.
22. H.E.S. Fath, S.M. Elsherbiny, A.A. Hassan, M. Rommel, M. Wieghaus, J. Koschikowski, et al., PV and thermally driven small-scale, stand-alone solar desalination systems with very low maintenance needs, Desalination 225 (2008) 58–69.
23. A.A. ElDifrawi, C.F. Blazek, B.D. Yudow, US4363703 Thermal gradient humidification-dehumidification desalination system, 1982.
24. W.E. Sear, US4172767 Water purification system, 1979.
25. B.W. Hanning, US4187151 Apparatus for producing sweet water, 1980.
26. D. Zarzo, D. Prats, Desalination and energy consumption – what can we expect in the near future, Desalination 427 (2018) 1-9.

27. S. Jamaly, N.N. Darwish, I. Ahmed, S.W. Hasan, A short review on reverse osmosis pretreatment technologies, Desalination 354 (2014) 30–38.
28. D.A. Roberts, E.L. Johnston, N.A. Knott, Impacts of desalination plant discharges on the marine environment: a critical review of published studies, Water Res. 44 (2010) 5117–28.
29. J. Morillo, J. Usero, D. Rosado, H. El Bakouri, A. Riaza, F.J. Bernaola, Comparative study of brine management technologies for desalination plants, Desalination 336 (2014) 32–49.
30. A. Shahmansouri, J. Min, L. Jin, C. Bellona, Feasibility of extracting valuable minerals from desalination concentrate: a comprehensive literature review, J. Clean. Prod. 100 (2015) 4–16.
31. H. SharonK, K.S. Reddy, A review of solar energy driven desalination technologies, Renewable and Sustainable Energy Reviews, 41 (2015) 1080-118.
32. C. Li, Y. Goswami, E. Stefanakos, Solar assisted sea water desalination: A review. Renew. Sustain. Energy Rev. 19 (2013) 136–63.
33. C.S. Turchi, S. Akar, T. Cath, J. Vanneste, Use of low-temperature geothermal energy for desalination in the Western United States, Technical Report NREL/TP-5500-65277, November 2015. Available online at: http://www.nrel.gov/docs/fy16osti/65277.pdf.
34. K.T.L. Bourouni, J.C. Deronzier, Experimentation and modelling of an innovative geothermal desalination unit, Desalination 125 (1999) 147–53.
35. J. Leijon, C. Boström, Freshwater production from the motion of ocean waves – A review, Desalination 435 (2018) 161–71.
36. P.A. Davies, Wave-powered desalination: resource assessment and review of technology, Desalination 186 (2005) 97–109.
37. S. Sarp, N. Hilal, Membrane-based salinity gradient processes for water treatment and power generation, 1st Ed (2018) Elsevier.
38. A. Sadeghpour, Z. Zeng, H. Ji, N. Dehdari Ebrahimi, A.L. Bertozzi, Y.S. Ju, Water vapor capturing using an array of traveling liquid beads for desalination and water treatment, Science Advances 5 (2019) eaav7662.
39. Michell Instruments, Humidity Calculator, http://www.michell.com/us/calculator/, last accessed on 02/01/2019.
40. ASHRAE, 2017 ASHRAE Handbook – Fundamentals, Har/Cdr edition, ASHRAE, 2017,
41. X. Ji, Thermodynamic properties of humid air and their application in advanced power generation cycles, Doctoral Dissertation, KTH-Royal Institute of Technology, 2006.

42. M.J. Moran, H. N. Shapiro, Fundamentals of Engineering Thermodynamics, 8th edition, John Wiley & Sons, 2014.
43. Z.K. Morvay, D.D. Gvozdenac, Applied Industrial Energy and Environmental Management, John Wiley & Sons, 2009.
44. F. White, Fluid Mechanics, 8th edition, McGraw-Hill Education, 2015.